3-1999

Mid-Infrared Visibility Measurements of Evolved Stars

Jeffrey J. Sudol
West Chester University of Pennsylvania, jsudol@wcupa.edu

H. M. Dyck
University of Wyoming

R. E. Stencel
University of Denver

D. I. Klebe
University of Denver

M. J. Creech-Eakman
University of Denver

THE ASTRONOMICAL JOURNAL, 117:1609–1615, 1999 March

MID-INFRARED VISIBILITY MEASUREMENTS OF EVOLVED STARS

J. J. SUDOL[1] AND H. M. DYCK[2]
Department of Physics and Astronomy, University of Wyoming, P.O. Box 3905, Laramie, WY 82071

AND

R. E. STENCEL, D. I. KLEBE, AND M. J. CREECH-EAKMAN[3]
Department of Physics and Astronomy, Denver University, 2112 East Wesley Avenue, Room 212, Denver, CO 80208-0202
Received 1998 September 17; accepted 1998 December 7

ABSTRACT

We have used Denver University's Ten-and-Twenty Micron Camera at the Wyoming Infrared Observatory to image 12 evolved stars at 11.5 μm. We have obtained both visibility data and photometric magnitudes from these images. We have partially resolved the circumstellar dust shell for eight of these 12 stars: α Ori, VY CMa, IRC +10216, χ Cyg, IK Tau, NML Cyg, μ Cep, and IRC +10420. We compare our data to published data and to visibility curves predicted by radiative transfer models in the literature.

Key words: circumstellar matter — stars: AGB and post-AGB — stars: mass loss

1. INTRODUCTION

Many evolved stars are known to have circumstellar envelopes of gas and dust (Gehrz & Wolf 1971; Stencel, Pesce, & Bauer 1989; Young, Phillips, & Knapp 1993). The effort to determine the grain chemistry of the circumstellar dust and the mass-loss rates of the evolved stars spans several decades, from early work on R CrB (Loreta 1934; O'Keefe 1939) and α Her (Deutsch 1956) to the work currently being conducted at the Infrared Spatial Interferometer (Danchi et al. 1994; Bester et al. 1996; Hale et al. 1997; Monnier et al. 1997). The reason for such effort is that the chemical abundances of the galaxy strongly depend on the mass-loss process. Evolved stars are responsible for converting hydrogen and helium into heavier elements and depositing those elements into the interstellar medium through the mass-loss process. Evolved stars provide the material out of which future generations of stars and planets form (Bedijn 1988; Young et al. 1993).

To determine the grain chemistry of the circumstellar dust and estimate the mass-loss rates of the evolved stars, we must at present construct dust shell models. Such models require the specification of several parameters such as the inner radius of the dust shell (or the radius at which dust condensation begins), the temperature of the dust at the inner radius, the density of the dust at the inner radius, the temperature profile, the density profile, grain absorption efficiency, grain size, optical depth, and the luminosity of the parent star. The parameters of the dust shell model are modified to match observations of the infrared flux (Rowan-Robinson 1980; Marengo et al. 1997) or to match the spatial structure of the dust shell as revealed by interferometry (Danchi et al. 1994). In this paper, we focus on the latter effort.

The highest resolution observations made with the Infrared Spatial Interferometer (ISI) have been used to model, and in some cases infer dynamic changes in, circumstellar dust shells. The models rely almost solely on sparse, high spatial frequency visibility data, from 0.65 to 12 cycles arcsec^{-1}. The need for low spatial frequency data as a necessary check on the validity of the models motivated this research. We present in this paper 11.5 μm visibility data for α Ori, VY CMa, IRC +10216, χ Cyg, IK Tau, NML Cyg, μ Cep, IRC +10420, o Cet, TX Cam, R Cas, and CIT 3, adding significantly to the body of visibility data currently available to which many dust shell models are fitted. In § 2, we briefly discuss the instrumentation and present the circumstances of the observations. In § 3, we discuss the method by which we obtain visibility data from an array image. In § 4, we compare our observations to the visibility data available in the literature and visibility curves predicted by the circumstellar dust shell models constructed by Danchi et al. (1994), Bester et al. (1996), Hale et al. (1997), and Monnier et al. (1997). In § 5, we close with some discussion of the need and the possibilities for coeval and complete spatial frequency coverage from 0 to ~3.5 cycles arcsec^{-1}. Such data would allow for the construction of more accurate models of circumstellar dust than presently possible.

2. OBSERVATIONS

Between 1996 December and 1997 September, we obtained images of 12 of the brightest evolved stars at a wavelength of 11.5 μm with Denver University's Ten-aNd-Twenty micron CAMera (TNTCAM) at the 2.3 m Wyoming Infrared Observatory (WIRO). These stars are listed in Table 1. All of the stars are variable in nature, so the date of observation and (if available) phase, ϕ, also appear in Table 1.

TNTCAM utilizes a liquid helium–cooled Rockwell HF-16 128 × 128 Si:As array (Klebe, Dahm, & Stencel 1996). The plate scale for TNTCAM is 0.″5 pixel^{-1} at WIRO. The 11.5 μm filter is a silicate band filter with a 1.2 μm bandwidth. The Rayleigh diffraction limit at 11.5 μm at WIRO is 1.″26, which corresponds to a spatial frequency limit of 0.79 cycles arcsec^{-1}.

3. DATA REDUCTION

In the first stage of image processing, we remove the bad pixels and detector bias, account for the integration time,

[1] NASA Space Grant Fellow (1997–1998).
[2] Present address: US Naval Observatory, Astrometry Division, Navy Prototype Optical Interferometer, Rural Route 14, Box 447, Flagstaff, AZ 86001.
[3] Present address: Department of Physics and Astronomy, California Institute of Technology, MS 150-21, Pasadena, CA 91125.

TABLE 1

LOG OF OBSERVATIONS

Date	Source	Phase	Spectral Type	$m_{11.5}$
1996 Dec 10.....	IRC +10216	0.02	C	−7.00 (xx)
1997 Aug 08	o Cet	0.50	M7 III	−4.60 (16)
1997 Sep 13	α Ori	...	M1 I	−5.49 (06)
	VY CMa	...	M3 II	−6.34 (06)
	IK Tau	...	M6 III	−5.55 (06)
1997 Sep 14	TX Cam	0.60	M8 III	−3.67 (06)
	CIT 3	...	M9 III	−4.05 (06)
1997 Sep 15	NML Cyg	...	M6 III	−5.57 (06)
	IRC +10420	...	F8 Ia	−4.25 (06)
1997 Sep 17	χ Cyg	0.96	S	−4.48 (06)
	μ Cep	0.45	M2 I	−4.23 (06)
	R Cas	0.43	M7 III	−3.98 (06)

NOTES.—The magnitude of IRC +10216 is an estimate. The uncertainty in the magnitude appears in parentheses.

and subtract sky frames from source frames using standard IRAF software packages (Tody 1993). We do not flat-field the frames as is customary for array images. The instrument electronics introduce a noise pattern at the 2% level to the readout of the array, which changes slowly but persistently during an observing run. The noise pattern dominates over differences in pixel sensitivity across the array. Flat-fielding consequently has the effect of altering the noise pattern, not removing it. Visibility data generated from flat-fielded and non–flat-fielded images differ by a mean of 2% with the greatest differences occurring at the highest spatial frequencies. Photometric data generated from the same images differ by less than 0.1%.

In the second stage of image processing, we transform the two-dimensional array images into one-dimensional images that resemble those that would be obtained with a scanning slit speckle interferometer. We remove from each image a 64 × 64 pixel frame centered on the source. We average the pixel values in each column, reducing the frame to a single row. In order to account for noise, we also remove from each image two 32 × 64 pixel frames sufficiently far from the source such that the frames contain no information about the source. We merge these two frames to construct a single 64 × 64 pixel "noise" frame. Again, we average the pixel values in each column, reducing the frame to a single row. Each "source" frame therefore has a corresponding "noise" frame. We mount TNTCAM on the telescope such that the array rows/columns sample 0°/90° position angles with respect to north. By rotating each image 90° and repeating the image reduction process, we have one-dimensional images that sample both the north-south and east-west structures of a source.

To extract visibility data from these one-dimensional images, we first construct the power spectrum (the complex square of the Fourier transform) of each "source" frame and "noise" frame. We then subtract the noise from the source. We typically acquire 16 images per source, so we next average all of the noise-free power spectra with equal weighting. We then normalize the average to its DC component.

The result of the data reduction process to this point is the product of the square of the visibility of the source, which describes the true structure of the source, and the square of the modulation transfer function (MTF), which describes the artificial structure introduced into the image of the source by the imaging system. (The imaging system includes the atmosphere, the telescope, and the camera.) To arrive at the true structure of the source, we must remove the artificial structure. During the course of an observing run, we alternate between acquiring images of sources of scientific interest that we presume to have structure (extended sources) and sources that we presume to have no structure (point sources). The visibility of a point source is unity so the image of a point source provides a measure of the MTF. In the final step in the data reduction process, we divide the power spectrum of the image of an extended source by an average of several power spectra of point source images. The result is the square of the visibility of the extended source.

The following equation effectively summarizes the data reduction:

$$V(s) = \left[\frac{\langle I_e^2(s) - N_e^2(s)\rangle}{\langle I_e^2(0) - N_e^2(0)\rangle}\right]^{1/2}\left[\left\langle\frac{\langle I_p^2(s) - N_p^2(s)\rangle}{\langle I_p^2(0) - N_p^2(0)\rangle}\right\rangle\right]^{-1/2}, \quad (1)$$

where $V(s)$ is the visibility of an extended source at spatial frequency s, $I_e^2(s)$ is the power spectrum of an image of the source, $I_p^2(s)$ is the power spectrum of an image of a point source, and $N_e^2(s)$ and $N_p^2(s)$ are the power spectra of the noise associated with $I_e^2(s)$ and $I_p^2(s)$, respectively. The angle brackets represent the process of averaging data. The averaging process for the point source data deserves further discussion.

Typically in interferometry, a single observation of an extended source is normalized to a single observation of a point source. The observations occur in sequence, and the point source is typically no more than a few degrees from the extended source, so that significant changes in the MTF do not occur between the two observations. At 11.5 μm, point sources are so scarce that extended sources and point sources are often separated by a few tens of degrees. As a consequence of this great separation of sources on the sky, the stability of the imaging system is a serious concern. A change in the MTF between the observation of an extended source and the observation of a point source introduces a systematic error into the visibility of the extended source.

The MTF could change significantly if either the optical system or the atmospheric seeing conditions change between observations. We do not find any evidence that significant changes occurred in the optical system during our observations. We do find, though, that atmospheric seeing conditions had some influence on our observations.

If we choose a Fried parameter of $r_0 = 0.10$ m at 0.5 μm, and a wind velocity of 5 m s^{-1}, the atmospheric correlation time at 11.5 μm is 0.27 s (Tango & Twiss 1980). In order to avoid the degrading effects of the atmosphere on the MTF, as is typically done in speckle interferometry, integration times at 11.5 μm should be only a fraction of a second. A single image obtained with TNTCAM is the equivalent of a 10 s integration, a factor of $\sim$40 in excess of the integration times expected for speckle interferometry. Therefore, the MTF of our imaging system is subject to the effects of seeing, and the long-exposure MTF developed by Fried (1966) is the appropriate model for the MTF.

We obtained only one observation of a point source during the 1996 December observing run. We obtained six observations of various point sources over the course of one night during the 1997 August observing run, and we obtained eight observations of various point sources over the course of four nights during the 1997 September observing run. For each observing run, we have constructed a weighted average MTF from the point source observations. Modeling these with the long-exposure MTF gives the following values for r_0: 1996 December, $r_0 = 0.050$ m (3%); 1997 August, $r_0 = 0.084$ m (3%); 1997 September, $r_0 = 0.067$ m (6%), where all values for r_0 are given at 0.5 μm and the values in parentheses indicate the goodness of fit. We want to emphasize that these values for r_0 are minimum values because we did not fully characterize the optical system at the time of the observations. If we were to include static, optical aberrations in the model for the MTF, the values for r_0 would be larger than stated.

We have only one measurement of the MTF for the December observing run, so we cannot adequately assess the stability of the MTF at that time. The six measurements of the MTF during the August observing run agree with one another to within the scatter in the data. We conclude from this that no significant changes occurred in the atmospheric conditions during the August observing run. The eight measurements of the MTF during the September observing run do not agree with one another to within the scatter. The disagreement is slight, and we can account for this disagreement with a variation in r_0 of approximately $\pm 4\%$ at 11.5 μm. This suggests that slight changes in atmospheric conditions occurred between observations.

In view of these results, we have decided to use the weighted average of all of the point source visibilities to normalize the extended source visibilities within an observing run, as indicated in equation (1). This method differs from the traditional method of working with extended/point source pairs, though the traditional method is typically applied when extended/point source pairs are observed in rapid sequence and only a few degrees apart on the sky. One consequence of adopting this technique is that the September visibility data may contain systematic errors of a few percent.

We must note that although we expected to obtain two dimensions of structural information from the array images, we found it necessary to discard the one-dimensional images sampling north-south structure. A faulty analog-to-digital converter in the instrument electronics caused every 16th pixel in all of the images to "float" particularly high or low of the mean—sometimes imperceptibly, other times by several percent. The array readout is such that every 16th pixel in an image is separated by eight columns and two rows. In the integration of columns to create a one-dimensional image, this floating pixel separation corresponds to a low spatial frequency of 1 in 8 pixels, or 0.25 cycles arcsec^{-1}. After the rotation and integration operation, the floating pixel separation corresponds to a high spatial frequency of 1 in 2 pixels, or 1.0 cycles arcsec^{-1}. One subtle difficulty of the data reduction process is that a noise frame can never provide a perfect measure of the noise in the source frame because the noise frame must be constructed away from the source. The residual noise in the visibility data in part stems from this difficulty. The influence of the floating pixels is just strong enough in the images that sample north-south structure that we would rather not trust those images. However, the influence of the floating pixels is negligible in the images that sample east-west structure because the floating pixel spacing corresponds to a spatial frequency beyond the spatial frequency limit of the data.

In addition to obtaining visibility data from the images, we obtain photometric data. We only briefly summarize the process here, which is similar to the process of "tipping" used at millimeter wavelengths. Creech-Eakman (1997) gives a more complete description of the reduction process. We make a set of observations at the telescope over the course of the observing run to determine both the telescope emissivity and a correlation between the telescope temperature and the radiative emission of the atmosphere. This allows us to calculate the atmospheric transmissivity at the time of observation of each source. We calculate the atmospheric extinction from the transmissivity. We correct the detector counts for extinction, then convert the detector counts to a standard magnitude. Our standard magnitude calibration is based on the work of Cohen & Davies (1995). The photometric data from our observations appear in Table 1. The uncertainties in the photometric data are calculated from the scatter in the detector counts and the uncertainty in the standard magnitude calibration.

4. DISCUSSION OF RESULTS

For eight of the 12 sources observed, α Ori, VY CMa, χ Cyg, IRC +10216, IK Tau, NML Cyg, μ Cep, and IRC +10420, the dust shell is partially resolved. For the remaining four stars, o Cet, TX Cam, R Cas, and CIT 3, the dust shell is unresolved. In this section, we compare our 11.5 μm visibility data to published data and to model visibility curves from the literature for six of the eight resolved sources. We have included most but not all 11 μm visibility data from the literature.

α Ori.—In Figure 1, we present a comparison of our data for α Ori with data from Sutton et al. (1977), Howell, McCarthy, & Low (1981), Dyck & Benson (1992), Danchi et al. (1994, hereafter D94), and Bester et al. (1996, hereafter B96). For clarity, we have plotted data from D94 only for the observation period 1988 October–1989 October and data from B96 only for the observation period 1994 September 5–1994 October 12. We also plot the visibility curves predicted by the multiple, thin shell models from both D94 and B96.

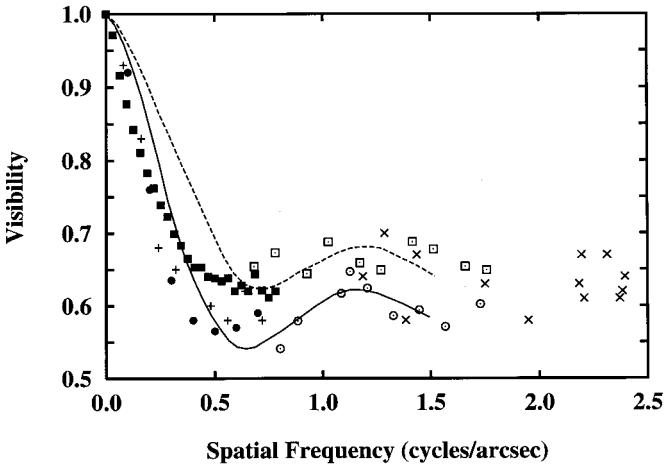

FIG. 1.—Visibility data and model visibility curves for α Ori. *Filled squares*: our data; *open circles*: data from Danchi et al. 1994; *open squares*: data from Bester et al. 1996; *filled circles*: data from Dyck & Benson 1992; *plus signs*: data from Howell et al. 1981; *crosses*: data from Sutton et al. 1977; *solid line*: double shell model from Danchi et al. 1994; *dashed line*: double shell model from Bester et al. 1996.

In Figure 1, we see two distinct data domains. At spatial frequencies less than 0.2 cycles arcsec^{-1}, there is little dispersion in the data over a time period of ~17 yr, from 1980 to 1997. At spatial frequencies greater than 0.5 cycles arcsec^{-1}, there is significant dispersion in the data over a comparable time period. To quantify this dispersion, we find that at 0.2 cycles arcsec^{-1}, $\Delta V = 0.03$, whereas at 1.0 cycles arcsec^{-1}, $\Delta V = 0.12$. Two fundamentally different models have been proposed to account for the observations.

Both Howell et al. and Dyck & Benson use a "Gaussian shell" model to account for their data. We have fitted such a model to our data as well. The Gaussian shell model uses a delta function to represent the brightness distribution of the stellar component and a symmetric, spherical Gaussian to represents the brightness distribution of the dust component. The model parameters are the ratio of the flux of the stellar component to the total flux of the system and the angular diameter of the dust shell. In Table 2, we present those model parameters (independently determined) that best fit each of the low spatial frequency data sets presented in Figure 1. We find the mean FWHM angular diameter of the dust shell to be 2.″5 ± 0.″1 and the mean ratio of the stellar flux to the total flux to be 63% ± 6%, where the uncertainty quoted is the rms scatter. The mean diameter is within the rms scatter of the individual determinations of the diameter. The same agreement does not hold for the flux ratio. The uncertainty in a single determination of the flux ratio is estimated to be ±3%, whereas the rms scatter of the mean flux ratio is ±6%.

TABLE 2

COMPARISON OF THE RESULTS OF INDEPENDENT GAUSSIAN SHELL MODEL FITS TO LOW SPATIAL FREQUENCY VISIBILITY DATA FOR α ORIONIS

Year	λ (μm)	FWHM (arcsec)	I_p/I_{tot}	References
1980	11.6	2.5 ± 0.2	0.69	1
1988–1989.....	11.4	2.4 ± 0.1	0.57	2
1997	11.5	2.6 ± 0.3	0.63	3

NOTES.— FWHM represents the angular diameter of the best-fit Gaussian-shell model. I_p/I_{tot} represents the ratio of the point source flux to the total flux.

REFERENCES.—(1) Howell et al. 1981; (2) Dyck & Benson 1992; (3) this paper.

We must note here that the Gaussian shell model is not a radiative transfer model. Nonetheless, Ridgway et al. (1986) have demonstrated that the Gaussian shell model is an excellent approximation to the spherical shell model in radiative transfer theory.

Both D94 and B96 use a multiple, thin shell model to account for their data, and particularly the fine structure, or "ripple," in the data. D94 and B96 both propose that the thin shells result from episodic bursts of mass loss from the parent star. This hypothesis is supported by spectroscopic observations by Honeycutt et al. (1980). D94 conclude that the α Ori system consisted of two thin shells at 1″ and 2″ from the parent star at the time of their observations. D94 also note that their model, when evolved backward in time with fixed shell expansion velocities, can account for the low spatial frequency data obtained by Howell et al., the only low spatial frequency data available at the time of their publication. B96 present a model in which two, thin shells exist at 0.″1 and 1.″0 but do not evolve that model to account for any of the low spatial frequency data in the literature.

We find it difficult to account for all of the available visibility data to date with these models. The Gaussian shell model simply cannot replicate the ripple in the high spatial frequency data. The multiple, thin shell model creates more dispersion in the visibilities at low spatial frequencies as the shells expand than is observed. It is possible that a multiple, thin shell model in which new dust shells are produced episodically could account for all of the visibility data to date. However, the constancy of the visibility profile at low spatial frequencies does not strike us as a coincidence of the timing of observations and the particular state of evolution of the α Ori system. The data seem to demand components of both models.

We propose that steady mass loss sustains an extended dust shell. Episodic bursts in the mass loss produce density enhancements in the dust shell in thin regions that travel outward from the star. To test this hypothesis, we have constructed a model that uses a delta function to represent the brightness distribution of the stellar component and a combination of a spherically symmetric, Gaussian and two, infinitesimally thin, concentric rings to represent the brightness distribution of the dust component. In the best-fit model to our data alone, the stellar component contributes 77% of the total flux. The extended shell has a FWHM angular diameter of 1.″5 and contributes 20% of the total flux. The thin shell radii are 1″ and 2″, and the shells contribute 2.3% and 0.7% of the total flux, respectively. If we "evolve" this model simply by changing the shell radii each over a range of ±0.″25, which corresponds roughly to the change in the radius of a thin shell expanding at a rate of 20 km s^{-1} over two decades at a distance of 160 pc, we find $\Delta V = 0.03$ at 0.2 cycles arcsec^{-1} and $\Delta V = 0.11$ between 1.0 and 1.5 cycles arcsec^{-1}, in good agreement with the observed dispersion in the data.

The model we have constructed, like the Gaussian shell model, is not a radiative transfer model but rather involves a direct transform of a function that approximates the

brightness distribution of the source into a visibility curve. A radiative transfer model is beyond the scope of this paper. One must interpret the model we have constructed with some caution, but we find it encouraging for our hypothesis that the model has the qualitative properties of the data: ripple in the visibility profile at high spatial frequencies and the combination of low dispersion in visibility at low spatial frequencies and high dispersion in the visibilities at high spatial frequencies as the model evolves.

VY CMa.—In Figure 2, we present a comparison of our data for VY CMa with data from Sutton et al. (1977) and data from D94 at maximum and minimum light. We also present the visibility curves predicted by the maximum and minimum luminosity models from D94.

A smooth curve through our data and continuing through the data from Sutton et al. qualitatively follows the model curves but is systematically low. This suggests that the models do not encompass the full range of the variation of the visibility profile of the source. As a note of interest, the AAVSO visible light curve for VY CMa shows regular fluctuations between 1985 and 1995 with an approximate period of 1500 days. All of the observations made at the ISI occur at the maxima and minima of these regular fluctuations. A disruption in this regular behavior appears just prior to our observations.

χ Cyg.—In Figure 3, we present our data for χ Cyg at $\phi = 0.96$ and data from D94 at $\phi = 0.35$ and at $\phi = 0.88$. Our data agree best with the high- and low-temperature, silicate-graphite mix models from D94, also presented in Figure 3, but the scatter in our data does not allow us to say anything more conclusive.

IRC +10216.—In Figure 4, we present a comparison of our data for IRC +10216 with data from D94 at maximum and minimum light. We also present the "alternate" maximum and minimum luminosity models from D94. According to light curve data reported by Dyck et al. (1991), we observed IRC +10216 at $\phi = 0.02$, and our data do tend to blend with the data from D94 obtained at $\phi = 0$. As with χ Cyg, though, the scatter in our data limits the sense of agreement with the models.

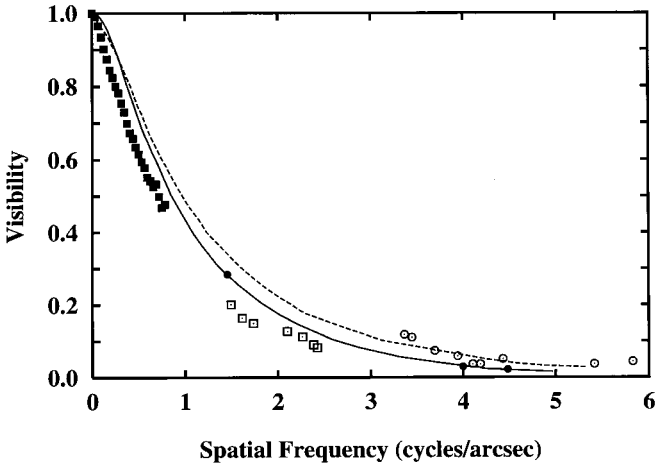

FIG. 2.—Visibility data and model visibility curves for VY CMa. *Filled squares*: our data; *open squares*: Sutton et al. 1977; *filled circles*: maximum luminosity data from Danchi et al. 1994; *open circles*: minimum luminosity data from Danchi et al. 1994; *solid line*: maximum luminosity model from Danchi et al. 1994; *dashed line*: minimum luminosity model from Danchi et al. 1994.

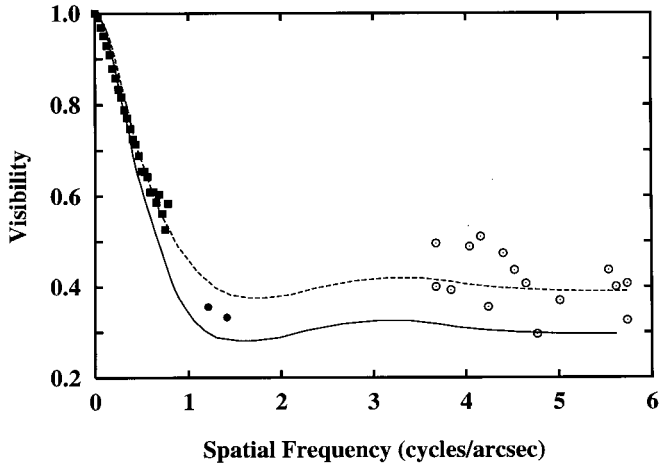

FIG. 3.—Visibility data and model visibility curves for χ Cyg. *Filled squares*: our data; *open circles*: data from Danchi et al. 1994 at $\phi = 0.35$; *filled circles*: data from Danchi et al. 1994 at $\phi = 0.88$; *solid line*: silicate-graphite mix, high-temperature model from Danchi et al. 1994; *dashed line*: silicate-graphite mix, low-temperature model from Danchi et al. 1994.

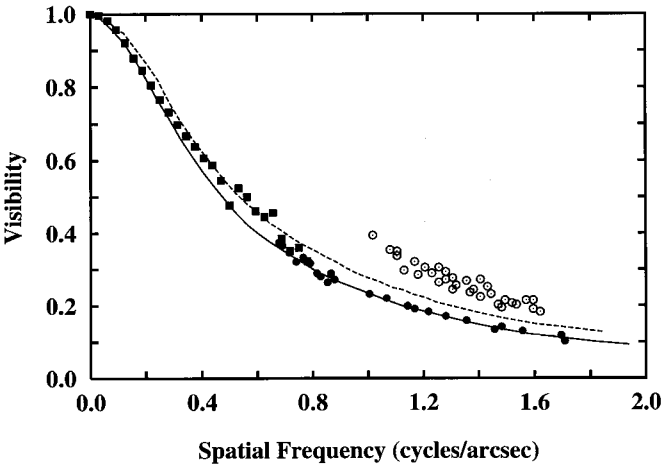

FIG. 4.—Visibility data and model visibility curves for IRC +10216. *Filled squares*: our data; *filled circles*: maximum luminosity data from Danchi et al. 1994; *open circles*: minimum luminosity data from Danchi et al. 1994; *solid line*: "alternate" maximum luminosity model from Danchi et al. 1994; *dashed line*: "alternate" minimum luminosity model from Danchi et al. 1994.

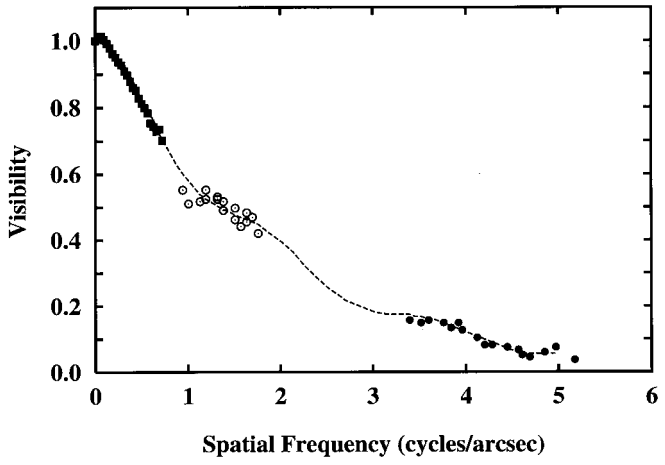

FIG. 5.—Visibility data and model visibility curves for IK Tau. *Filled squares*: our data; *filled circles*: data from Danchi et al. 1994; *open circles*: data from Hale et al. 1997; *dashed line*: double shell model from Hale et al. 1997.

IK Tau.—In Figure 5, we present a comparison of our data with data from D94 and Hale et al. (1997, hereafter H97). We also present the visibility curve predicted by the double shell model from H97. We find excellent agreement between our data and the model!

NML Cyg.—In Figure 6, we present a comparison of our data with data from Dyck & Benson (1992) and Monnier et al. (1997, hereafter M97). We also present the visibility curve predicted by the mean temperature, mean luminosity, double shell model from M97. In the legend for Figure 6, we have noted the dates and the position angles of the observations.

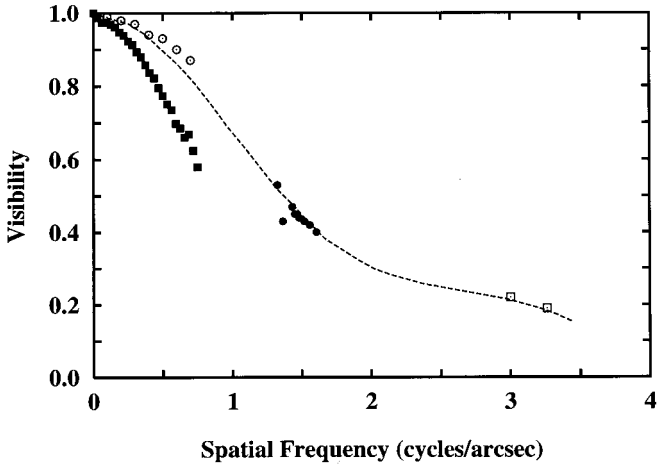

FIG. 6.—Visibility data and model visibility curves for NML Cyg. *Filled squares*: our data from 1997 observations at a position angle of 90°; *open squares*: data from 1993 observations at position angles of 93° and 97° from Monnier et al. 1997; *filled circles*: data from 1994–1996 observations at position angles ranging from 50° to 70° from Monnier et al. 1997; *open circles*: 1988–1989 observations at a position angle of 0° from Dyck & Benson 1992; *dashed line*: double shell model from Monnier et al. 1997.

In view of the trend in the data with date of observation, one could argue that the circumstellar envelope, regardless of its geometry, is expanding. In such an instance, evolution of the M97 model could account for all of the 11 μm visibility data to date. In view of the trend in the data with position angle, one could argue that the circumstellar envelope is highly asymmetric. Dyck, Forbes, & Shawl (1971) have reported strong polarization at optical and infrared wavelengths for NML Cyg, which suggests the dust envelope is asymmetric. Richards, Yates, & Cohen (1996) convincingly argue that the OH and H_2O structures associated with NML Cyg trace a bipolar outflow. The 11 μm data do not conclusively point to either an expanding, double shell model or to a bipolar model. Coeval visibility data for NML Cyg over a minimum of three position angles and over a range of 0 to $\sim$3.5 cycles arcsec^{-1} are needed to resolve this issue.

μ Cep and IRC +10420.—No high spatial frequency data have been published for either μ Cep or IRC +10420. We present the visibility data for μ Cep and IRC +10420 along with the data for α Ori, VY CMa, χ Cyg, IRC +10216, IK Tau, and NML Cyg in Table 3. We have not included error bars in the figures for the sake of clarity; instead, we present the uncertainty data in Table 3. The first component of the uncertainty is the standard deviation of the mean associated with the first term in equation (1). The second component of the uncertainty is the standard deviation of the weighted mean associated with the second term in equation (1).

TABLE 3

VISIBILITY DATA FOR EIGHT OF THE 12 STARS OBSERVED IN THIS RESEARCH

s	α Ori	VY CMa	IRC +10216	χ Cyg	IK Tau	NML Cyg	μ Cep	IRC +10420
0.00000.....	1.00 (01)	1.00 (01)	1.00 (06)	1.00 (01)	1.00 (02)	1.00 (01)	1.00 (02)	1.00 (01)
0.03125.....	0.97 (01)	0.99 (01)	1.00 (08)	0.99 (01)	1.01 (02)	0.99 (01)	0.98 (02)	0.98 (01)
0.06250.....	0.92 (01)	0.97 (01)	0.98 (08)	0.97 (01)	1.01 (02)	0.97 (01)	0.95 (02)	0.96 (01)
0.09375.....	0.88 (01)	0.93 (01)	0.96 (08)	0.95 (01)	1.00 (02)	0.97 (01)	0.93 (02)	0.93 (01)
0.12500.....	0.84 (01)	0.90 (01)	0.92 (08)	0.93 (01)	0.99 (02)	0.97 (01)	0.91 (02)	0.90 (01)
0.15625.....	0.81 (01)	0.87 (01)	0.88 (08)	0.91 (02)	0.98 (02)	0.96 (01)	0.89 (02)	0.88 (01)
0.18750.....	0.78 (01)	0.84 (01)	0.85 (07)	0.88 (02)	0.96 (02)	0.95 (01)	0.86 (02)	0.84 (01)
0.21875.....	0.76 (01)	0.82 (01)	0.80 (07)	0.86 (03)	0.95 (03)	0.94 (02)	0.85 (03)	0.82 (01)
0.25000.....	0.74 (01)	0.80 (02)	0.77 (07)	0.83 (03)	0.94 (03)	0.92 (02)	0.82 (03)	0.79 (02)
0.28125.....	0.72 (02)	0.78 (02)	0.73 (07)	0.82 (04)	0.93 (03)	0.91 (03)	0.80 (03)	0.77 (02)
0.31250.....	0.70 (02)	0.75 (02)	0.70 (07)	0.79 (04)	0.91 (04)	0.89 (03)	0.78 (04)	0.74 (02)
0.34375.....	0.68 (02)	0.73 (02)	0.67 (07)	0.77 (05)	0.90 (04)	0.88 (04)	0.76 (04)	0.72 (02)
0.37500.....	0.67 (02)	0.70 (03)	0.64 (07)	0.75 (05)	0.88 (04)	0.86 (04)	0.74 (04)	0.69 (03)
0.40625.....	0.65 (02)	0.67 (03)	0.61 (07)	0.73 (06)	0.86 (05)	0.84 (05)	0.71 (05)	0.67 (03)
0.43750.....	0.65 (02)	0.66 (03)	0.59 (08)	0.71 (06)	0.85 (05)	0.82 (05)	0.70 (05)	0.66 (03)
0.46875.....	0.64 (03)	0.63 (03)	0.54 (08)	0.69 (06)	0.83 (06)	0.80 (05)	0.68 (05)	0.64 (03)
0.50000.....	0.64 (03)	0.61 (04)	0.48 (09)	0.65 (07)	0.81 (06)	0.77 (06)	0.66 (06)	0.63 (04)
0.53125.....	0.63 (03)	0.59 (04)	0.52 (09)	0.65 (07)	0.80 (06)	0.75 (06)	0.65 (06)	0.59 (04)
0.56250.....	0.64 (04)	0.58 (04)	0.50 (09)	0.64 (07)	0.78 (07)	0.73 (07)	0.63 (06)	0.58 (04)
0.59375.....	0.62 (04)	0.55 (04)	0.46 (09)	0.61 (07)	0.75 (07)	0.70 (07)	0.61 (07)	0.56 (04)
0.62500.....	0.63 (05)	0.54 (05)	0.45 (10)	0.61 (07)	0.74 (07)	0.69 (07)	0.59 (07)	0.57 (05)
0.65625.....	0.62 (05)	0.53 (05)	0.46 (10)	0.59 (07)	0.73 (08)	0.66 (08)	0.57 (07)	0.56 (05)
0.68750.....	0.64 (05)	0.53 (06)	0.38 (09)	0.60 (08)	0.74 (08)	0.67 (08)	0.58 (08)	0.59 (06)
0.71875.....	0.62 (06)	0.50 (06)	0.35 (11)	0.56 (08)	0.70 (09)	0.62 (08)	0.53 (08)	0.54 (06)
0.75000.....	0.61 (06)	0.47 (07)	0.36 (13)	0.53 (07)	0.68 (09)	0.58 (08)	0.48 (08)	0.52 (07)
0.78125.....	0.62 (08)	0.48 (09)	0.32 (17)	0.58 (11)	0.77 (11)	0.62 (10)	0.51 (10)	0.56 (11)

NOTES.—The spatial frequency, s, is given in cycles per arcsecond. Uncertainties appear in parentheses.

o Cet, TX Cam, R Cas, and CIT 3.—We resolved no structure in *o* Cet, TX Cam, R Cas, and CIT 3. This is not to suggest that no circumstellar dust shells are associated with these sources; rather, our observations suggest that the circumstellar dust shells for these sources have angular diameters on the order of or less than 0.″63. We note that TX Cam, R Cas, and CIT 3 are the three faintest sources observed, in that order.

5. CONCLUSION

We have obtained photometric data and visibility data for 12 evolved stars from array images at 11.5 μm. We have partially resolved the circumstellar dust shell of eight of the 12 stars: α Ori, VY CMa, IRC +10216, χ Cyg, IK Tau, NML Cyg, μ Cep, and IRC +10420. The models in the literature for the α Ori system do not adequately account for all of the visibility data obtained over the past two decades. We propose that steady mass loss sustains an extended structure and that episodic outbursts result in density variations in that structure.

Our visibility data for VY CMa, IRC +10216, χ Cyg, and IK Tau agree well with published data and with specific radiative transfer models as given in this paper. Our visibility data for NML Cyg, on the other hand, do not agree with previously published data. Although not conclusive, the data are consistent with a bipolar outflow model. We have also provided new visibility data for μ Cep and IRC +10420.

The mid-infrared region is certainly the region of choice for studying the structure of circumstellar dust shells. In review of the work done at 11 μm to date, we see a need for coeval observations which completely cover spatial frequencies from 0 to $\sim$3.5 cycles arcsec^{-1}. Such observations could be made with either a speckle-mode mid-infrared camera at a 10 m class telescope or a three-baseline mid-infrared interferometer (to cover high spatial frequencies) working in conjunction with an imaging mode mid-infrared camera at a meter-class telescope (to cover low spatial frequencies).

This research has been funded in part by NSF grant AST-9528129, The Wyoming Space Grant Consortium and NASA, The Paul Stock Fund, The Research Office of the University of Wyoming, and The Department of Physics and Astronomy of the University of Wyoming. We would like to thank Ron Canterna for providing a portion of the observing time at WIRO, and R. Howell and James Weger for statistics and facts about WIRO. We would like to acknowledge the assistance of Mark Huber, Renee Saxton, Matt Rivett, Catherine Boone, Mark Welegala, Mike Fitz, Matti Jalakas, Mike Read, and Neeharika Thakur. In this research, we have used, and acknowledge with thanks, data from the AAVSO International Database, based on observations submitted to the AAVSO by variable star observers worldwide. We have also made use of the SIMBAD database maintained by the CDS, Strasbourg, France.

REFERENCES

Bedijn, P. J. 1988, A&A, 205, 105
Bester, M., Danchi, W. C., Hale, D., Townes, C. H., Degiacomi, C. G., Mekarnia, D., & Geballe, T. R. 1996, ApJ, 463, 336
Cohen, M., & Davies, J. K. 1995, MNRAS, 276, 715
Creech-Eakman, M. J. 1997, Ph.D. thesis, Denver Univ.
Danchi, W. C., Bester, M., Degiacomi, C. G., Greenhill, L. J., & Townes, C. H. 1994, AJ, 107, 1469
Deutsch, A. J. 1956, ApJ, 123, 210
Dyck, H. M., & Benson, J. A. 1992, AJ, 104, 377
Dyck, H. M., Benson, J. A., Howell, R. R., Joyce, R. R., & Leinert, C. 1991, AJ, 102, 200
Dyck, H. M., Forbes, R. R., & Shawl, S. J. 1971, AJ, 76, 901
Fried, D. L. 1966, J. Opt. Soc. Am., 56, 1372
Gehrz, R. D., & Woolf, N. J. 1971, ApJ, 165, 285
Hale, D. D. S., et al. 1997, ApJ, 490, 407
Honeycutt, R. K., Bernat, A. P., Kephart, J. E., Gow, C. E., Sandford, M. T., II, & Lambert, D. L. 1980, ApJ, 239, 565
Howell, R. R., McCarthy, D. W., & Low, F. J. 1981, ApJ, 251, L21
Klebe, D. I., Dahm, M. A., & Stencel, R. E. 1996, in ASP Conf. Ser. 97, Polarimetry of the Interstellar Medium, ed. W. G. Roberge & D. C. B. Whittet (San Francisco: ASP), 79
Loreta, E. 1934, Astron. Nach., 254, 151
Marengo, M., Canil, G., Silvestro, G., Origlia, L., Busso, M., & Persi, P. 1997, A&A, 322, 924
Monnier, J. D., et al. 1997, ApJ, 481, 420
O'Keefe, J. A. 1939, ApJ, 90, 294
Richards, A. M. S., Yates, J. A., & Cohen, R. J. 1996, MNRAS, 282, 665
Ridgway, S. T., Joyce, R. R., Connors, D., Pipher, J. L., & Dainty, C. 1986, ApJ, 302, 662
Rowan-Robinson, M. 1980, ApJS, 44, 403
Stencel, R. E., Pesce, J. E., & Bauer, W. H. 1989, AJ, 97, 1120
Sutton, E. C., Storey, J. W. V., Betz, A. L., & Townes, C. H. 1977, ApJ, 217, L97
Tango, W. J., & Twiss, R. Q. 1980, Prog. Opt., 17, 239
Tody, D. 1993, in ASP Conf. Ser. 52, Astronomical Data Analysis Software and Systems II, ed. R. J. Hanisch, R. J. V. Brissenden, & J. Barnes (San Francisco: ASP), 173
Young, K., Phillips, T. G., & Knapp, G. R. 1993, ApJ, 409, 725